PAPER

Check for updates

A dithieno[3,2-a:3',2'-j][5,6,11,12]chrysene diimide based polymer as an electron transport layer for efficient inverted perovskite solar cells†

Jintao Huang,[a] Congwu Ge,*[a] Fei Qin,[b] Jianwei Zhang,[c] Xiaodi Yang,[c] Ye Zou,[d] Yinhua Zhou, [iD][b] Wei-Shi Li [iD][a] and Xike Gao [iD]*[a]

The electron transport layer (ETL) plays an important role in promoting both photovoltaic performance and stability of perovskite solar cells (PSCs). n-Type conjugated polymers have been developed to replace the widely explored phenyl-C61-butyric acid methyl ester (PCBM) as an ETL, especially in p-i-n inverted planar PSCs, owing to their high-quality film features and excellent electron transport ability. Herein, a series of electron-deficient conjugated polymers (P(DTCDI-T), P(DTCDI-2T) and P(DTCDI-3T)) consisting of dithieno[3,2-a:3',2'-j][5,6,11,12]chrysene diimides (DTCDI) and different thiophene based units (thiophene (T), 2,2'-bithiophene (2T) and 2,2':5',2''-terthiophene (3T)) are reported as effective ETLs for inverted PSCs. Compared to control devices based on the PCBM ETL, these polymer-based devices display better photovoltaic performance, which is mainly due to the optimized electron extraction and transport properties of these DTCDI-based polymers, resulting in a champion power conversion efficiency (PCE) of 17.88% for P(DTCDI-2T) ETL based devices. Moreover, thanks to better film features, more effective interfacial passivation, lower trap-state density and hydrophobicity, these polymeric ETL based devices exhibit considerably improved stability.

Introduction

Perovskite solar cells (PSCs) have exhibited their great charms in the potential promotion of power conversion efficiency (PCE) over the past decade, owing to the superb light-harvesting ability, long balanced charge-carrier diffusion length, and high carrier mobility of the perovskite layer.[1–8] High-performance PSCs are often planar device architectures prepared by inserting a perovskite layer between the electron transport layer (ETL) and hole transport layer (HTL).[9] In a PSC device, ETL and HTL play the critical role of selectively extracting the corresponding charge carrier and respectively transporting it to the cathode and anode. Thus, to obtain efficient PSCs, ETL and HTL are

required to fulfill (1) matched energy levels with the conduction band (CB) and valence band (VB) of the perovskite layer to minimize open circuit voltage (V_{OC}) loss, (2) good charge carrier selectivity to enhance charge extraction efficiency, and (3) high charge mobility to reduce carrier transport resistance loss.[10–12] A large number of HTLs have been developed to enhance hole collection efficiency.[13–19] However, the choice of ETLs is relatively limited, especially for inverted p-i-n type planar devices.[20] To date, fullerenes and their derivatives, particularly, phenyl-C61-butyric acid methyl ester (PCBM), are the most used ETLs in inverted planar PSCs, due to their high electron mobility and suitable energy level.[21–23] In spite of their promising device performance, the inherent defects of fullerene ETLs, such as low solubility, poor film morphology and inferior ambient stability, significantly hinder their practical application.[24,25] Therefore, it is urgently desired to design and select novel ETLs for enabling high-performance inverted planar PSCs.

n-Type conjugated polymers, having a number of merits, such as tailorable optoelectronic structure, good film-forming property and structural stability, and photochemical stability, have been reported to be promising alternatives to PCBM as efficient ETLs. In 2015, an n-type polymer N2200 (Scheme 1) was firstly reported to be an ETL for PSCs by Wang *et al.*[26] Although the PCE of the PSC devices was only obtained to be about 8%, this work inspired the research of n-type polymeric ETLs.

[a] *Key Laboratory of Synthetic and Self-Assembly Chemistry for Organic Functional Molecules, Shanghai Institute of Organic Chemistry, University of Chinese Academy of Sciences, Chinese Academy of Sciences, Shanghai 200032, China. E-mail: gecongwu@sioc.ac.cn, gaoxk@mail.sioc.ac.cn*

[b] *Wuhan National Laboratory for Optoelectronics, Huazhong University of Science and Technology, Wuhan, 430074, China*

[c] *The Research Center of Chiral Drugs, Innovation Research Institute of Traditional Chinese Medicine, Shanghai University of Traditional Chinese Medicine, 1200 Cailun Road, Shanghai 201203, China*

[d] *Beijing National Laboratory for Molecular Sciences, Key Laboratory of Organic Solids, Institute of Chemistry, CAS, Beijing 100190, China*

† Electronic supplementary information (ESI) available. See DOI: 10.1039/d1tc03942c

This journal is © The Royal Society of Chemistry 2022

J. Mater. Chem. C, 2022, **10**, 2703–2710 | **2703**

Scheme 1 Chemical structure of representative polymeric ETLs.

A breakthrough in polymeric ETLs for PSCs occurred when PFN-2TNDI was developed by Chen *et al.*[27] With amino-functionalized side chains, the PFN-2TNDI ETL can not only improve the surface passivation, but also reduce the work function of the cathode, and thus enhance the PCE to 16.7%. Later on, Tian *et al.* altered PFNDI's structure with fluoro- and amino- functionalized side chains, which improved the corresponding PSCs' performance to about 17.5%.[28] Zhang *et al.* introduced phosphite ester side chains into the PFNDI polymer to passivate the defects of the perovskite layer and the PSC devices acquired a PCE of 18.2%.[29] These efforts indicate that the side-chain functionalization strategy is an effective approach for molecular design of polymeric ETLs. Ahmed *et al.* used a donor–acceptor$_1$–donor–acceptor$_2$ (D–A$_1$–D–A$_2$) n-type NDI-based polymer as an ETL, but its-based PSCs' performance is relatively low because of an inappropriate HOMO level.[30] Kim *et al.* synthesized a D–A$_1$–D–A$_2$ type polymer P(NDI2DT-TTCN) with a deep-lying lowest unoccupied molecular orbital (LUMO) of −4.14 eV, which may help to improve the electron extraction efficiency, and PSCs based on P(NDI2DT-TTCN) achieved a PCE of 17%.[31] Jiang and coworkers employed a PDI-based conjugated polymer NDP-V as an ETL, and the corresponding PSCs showed PCE values of up to 16.5%.[32] Guo *et al.* reported two highly twisted bithiophene imide (BTI) based acceptor–acceptor (A–A) polymeric ETLs P(BTI-NDI) and P(BTI-PDI), and their based PSC devices exhibited a PCE of 19.5% and 20.8%, respectively.[33] Recently, they investigated two new homopolymers PBTI and PDTzTI, which are similar in chemical structure but different in LUMO energy level, allowing for the study of the effects of energy level on

device performance.[34] The PSC devices with PDTzTI ETL obtained a much higher PCE of up to 20.86% because of its matched energy level. This provides a guide for designing new ETLs for PSCs. These aforementioned achievements indicate that developing new polymeric ETLs offers a promising avenue to explore high-performance PSCs. Accordingly, to realize low-cost construction and long-term operation of high-performance PSC devices, an efficient ETL is expected to meet the following requirements: (i) good solubility, enabling solution processing fabrication, (ii) matched energy level alignment, facilitating electron extraction from the perovskite layer, (iii) capability of film-forming and adhesion on the perovskite surface, (iv) high electron mobility, ensuring efficient electron transport to the cathode, and (v) photo and thermal stability of its chemical structure and morphology over time.

Dithieno[3,2-*a*:3′,2′-*j*][5,6,11,12]chrysene diimide (DTCDI) is an electron-deficient twisted molecular backbone.[35] DTCDI-based small molecules and polymers have been explored in n-type organic field effect transistors and all-polymer solar cells, demonstrating promising device performance.[35,36] The DTCDI-3,9-connected polymer was found to have good solubility in commonly used solvents like tetrahydrofuran, methylene chloride and toluene. Meanwhile, uniform morphology feature was detected both in its neat and blend films, its electron mobility determined by the space-charge-limited current (SCLC) method is up to 10^{-4} cm^2 V^{-1} s^{-1} in blend film and the LUMO energy level was estimated to be −4.01 eV.[36] These properties demonstrate that the DTCDI-3,9-connected polymers are promising

2704 | *J. Mater. Chem. C*, 2022, **10**, 2703–2710

This journal is © The Royal Society of Chemistry 2022

candidates as efficient ETLs. It was reported that thiophene can effectively passivate the under-coordinated Pb^{2+} defects on the perovskite layer.[37] In this work, we copolymerized the DTCDI block from the 3,9-positions of chrysene with different thiophene moieties (thiophene, 2,2′-bithiophene and 2,2′:5′,2″-terthiophene) and obtained three donor–acceptor (D–A) type polymers P(DTCDI-T), P(DTCDI-2T) and P(DTCDI-3T), respectively. Their device performance as ETLs for inverted planar PSCs was evaluated and the performance of the control device with PCBM ETL was also investigated. The relationship between the ratio of thiophene units within the polymers and performance as ETLs was discussed *via* studies of film surface microstructure, optoelectronic properties and theoretical calculations. All three DTCDI-based polymers as ETLs for PSCs exhibited excellent electron extraction and transport properties, which outperformed PCBM. The inverted PSCs based on the P(DTCDI-T) ETL resulted in a preliminary PCE up to 15.75%, which is slightly higher than that of the PCBM based one (15.56%). It was found that an increase in the ratio of thiophene unit in the polymeric backbone favors the efficiency of electron extraction and reduces the resistance of interfacial charge transport. Enhanced PCEs of 17.88% and 17.74% were respectively achieved for P(DTCDI-2T) and P(DTCDI-3T) based devices. These results demonstrate that the DTCDI-3,9-connected polymers are hopeful efficient ETLs for constructing high-performance PSCs.

Results and discussion

Scheme 2 depicts the chemical structure of polymers P(DTCDI-T), P(DTCDI-2T) and P(DTCDI-3T), where DTCDI was used as the acceptor unit copolymerized with donor moieties thiophene (T), 2,2′-bithiophene (2T) and 2,2′:5′,2″-terthiophene (3T) *via* Stille cross-coupling reaction, respectively. The synthetic and purification procedure details of these polymers are displayed

Scheme 2 Synthesis of P(DTCDI-T), P(DTCDI-2T) and P(DTCDI-3T).

in the ESI.† The physicochemical properties of new polymers P(DTCDI-T) and P(DTCDI-3T), along with previously reported P(DTCDI-2T),[36] are summarized in Table 1. The thermal properties of these three polymers were evaluated by thermogravimetric analysis (TGA). They all exhibited good thermal stability with thermal decomposition temperatures (5% weight loss) of 410 °C, 452 °C and 436 °C (Fig. S1a, ESI†) for P(DTCDI-T), P(DTCDI-2T) and P(DTCDI-3T), respectively. Differential scanning calorimetry (DSC) measurements showed that both P(DTCDI-T) (Fig. S1b, ESI†) and P(DTCDI-2T) (Fig. S1c, ESI†) have an endothermic signal at about 280 °C, which is ascribed to the glass transition. However, no endothermic peak was found for the polymer P(DTCDI-3T) (Fig. S1d, ESI†).

The UV-vis absorption spectra of polymers P(DTCDI-T), P(DTCDI-2T) and P(DTCDI-3T) in dichloromethane solution and in spin-coated thin film are shown in Fig. 1a, and the data are collected in Table 1. All three polymers in dichloromethane solution showed two strong absorption bands, *i.e.* 350–460 nm and 460–750 nm for P(DTCDI-T), 350–480 nm and 480–750 nm for P(DTCDI-2T) and 350–535 nm and 535–750 nm for P(DTCDI-3T). The absorption maxima of P(DTCDI-T), P(DTCDI-2T) and P(DTCDI-3T) are at 615/393 nm, 605/402 nm and 665/476 nm in dichloromethane solution, and 617/393 nm, 636/412 nm and 658/449 nm in the film, and the optical band gaps obtained from the film absorption onset of P(DTCDI-T), P(DTCDI-2T) and P(DTCDI-3T) are 1.72 eV, 1.75 eV and 1.74 eV, respectively. The shorter wavelength feature is ascribed to the π–π* electronic transition, while the longer wavelength absorption band is attributed to one electron excitation from the HOMO to LUMO, reflecting photo-induced intramolecular charge transfer (ICT) between the electron-rich donor block and electron-deficient DTCDI unit within the polymeric chain.[39] Two vibronic peaks can be observed in the lower energy band, which is assigned to 0-0 and 0-1 vibronic transitions.[40] According to the literature, the 0-0 transition is related to the planarity of the polymer backbone within aggregates.[40–42] Therefore, an increase of 0-0/0-1 absorption ratio from P(DTCDI-T) to P(DTCDI-3T) correlates with the increased order of thin films.

Electrochemical properties of P(DTCDI-T), P(DTCDI-2T) and P(DTCDI-3T) were measured by cyclic voltammetry (CV) using ferrocene as the external standard. The corresponding CV curves are depicted in Fig. 1b. All of them exhibit quasi-reversible reduction and irreversible oxidation signals, and

Table 1 Optical and electrochemical properties of polymers P(DTCDI-T), P(DTCDI-2T) and P(DTCDI-3T)

Polymer	M_n (kDa)	PD	$\lambda_{max}{}^c$ [nm]		$E_g^{\text{opt } d}$ [eV]	$E_{LUMO}{}^e$ [eV]	$E_{HOMO}{}^e$ [eV]
			Solution	Film			
P(DTCDI-T)	8.4[a]	1.44[a]	391 615	393 617	1.72	−4.00	−6.39
P(DTCDI-2T)	15.1[b]	1.84[b]	399 605	412 636	1.75	−3.98	−6.14
P(DTCDI-3T)	12.2[b]	3.46[b]	475 661	449 658	1.74	−4.01	−6.04

[a] Measured from room-temperature gel permeation chromatography (GPC) *versus* polystyrene standard using tetrahydrofuran as the eluent. [b] Measured from high-temperature GPC at 140 °C *versus* polystyrene standard using dichlorobenzene as the eluent. [c] Absorption spectra of dichloromethane solution and film spin-coated from 5 mg mL^{-1} chloroform solution. [d] Estimated from absorption onset of the film using the equation $E_g^{\text{opt}} = 1240/\lambda_{\text{onset}}$ (eV). [e] Calculated from the equation $E_{LUMO} = -5.10$ eV $- E_{red}^{\text{onset}}$, $E_{HOMO} = -5.1$ eV $- E_{ox}^{\text{onset}}$, E_{red}^{onset} and E_{ox}^{onset} determined by cyclic voltammetry in 0.1 M $Bu_4N^+PF_6^-$ acetonitrile solution (*vs.* Fc/Fc$^+$).[38]

This journal is © The Royal Society of Chemistry 2022

J. Mater. Chem. C, 2022, **10**, 2703–2710 | **2705**

Fig. 1 (a) Optical absorption spectra of P(DTCDI-T), P(DTCDI-2T) and P(DTCDI-3T). (b) Cyclic voltammograms of P(DTCDI-T), P(DTCDI-2T) and P(DTCDI-3T) thin films measured in 0.1 M $Bu_4N^+PF_6^-$ acetonitrile solution with a scan rate of 100 mV s^{-1}.

the HOMO and LUMO energy levels were estimated to be $-6.39/$ -4.00 eV for P(DTCDI-T), $-6.14/-3.98$ eV for P(DTCDI-2T) and $-6.04/-4.01$ eV for P(DTCDI-3T), respectively.[38] Density functional theory (DFT) calculations of three repeat segments were also performed to understand these polymers' electronic properties. The variation trend of computed energy levels

Fig. 2 (a) Schematic illustration of the device configuration. (b) Band alignment of PSCs with different ETLs. (c) J–V curves of PSCs with different ETLs and (d) EQE spectrum. (e) J–V hysteresis of optimal PSCs with P(DTCDI-T), P(DTCDI-2T) and P(DTCDI-3T) ETLs under forward and reverse scan. (f) Device efficiency distribution with different ETLs.

(Fig. S2, ESI†) is −5.43/−3.21 eV, −5.25/−3.12 eV and −5.09/−3.16 eV for P(DTCDI-T), P(DTCDI-2T) and P(DTCDI-3T), respectively, in good agreement with that of the measured one. The electron density of the HOMO is averagely located in the molecular backbone for P(DTCDI-T). With increasing ratios of thiophene within the polymer chain, it is becomingly concentrated in thiophene moieties. The measured LUMO levels of the three polymers match well with the conduction band of the perovskite layer (−3.90 eV), which is beneficial for the electron extraction from the perovskite layer.[12] And the HOMOs are much deeper than the valence band of the perovskite film, which should prevent charge recombination at the corresponding interface due to efficient hole blocking.

To investigate the electron-transporting properties of the synthesized polymers, we constructed the electron-only devices with the structure of ITO/ZnO/ETL/Al, and the electron mobility (μ_e) was estimated by the space charge-limited current (SCLC) method (Fig. S3, ESI†). The obtained μ_e values for PCBM, P(DTCDI-T), P(DTCDI-2T) and P(DTCDI-3T) were 6.02×10^{-5}, 3.05×10^{-4}, 3.88×10^{-4} and 1.04×10^{-4} cm^2 V^{-1} s^{-1}, respectively. These polymers yield decent electron mobility, which is higher than or comparable to that of PCBM.

Further investigations on P(DTCDI-T), P(DTCDI-2T) and P(DTCDI-3T) as an ETL for PSCs were performed. Inverted planar perovskite solar cell devices with a structure of ITO/PTAA/MAPbI$_3$/ETL/BCP/Ag (Fig. 2a) were fabricated, where PTAA worked as the HTM, and BCP as the hole blocking layer. Fig. 2b illustrates the band alignment of PSCs with different ETLs. The fabrication details of PSCs can be found in the ESI.† The J–V curves are shown in Fig. 2c, and the corresponding photovoltaic performance parameters are collected in Table 2. Reference devices using PCBM as an ETL were also prepared, giving a champion PCE of 15.56%, a V_{OC} of 1.08 V, a J_{SC} of 19.80, and a FF of 72.95%. The P(DTCDI-T) based devices achieved slightly higher efficiency (15.75%) than the PCBM based one because of its superior short-circuit current density J_{SC}, though a lower FF. The devices with P(DTCDI-2T) and P(DTCDI-3T) ETLs achieved better performance with a PCE of 17.88% for P(DTCDI-2T), and 17.74% for P(DTCDI-3T), due to their improved FF. Fig. 2d shows the external quantum efficiency (EQE) variation of different ETLs, which is in accordance with the PCE trend. All polymeric ETL based devices exhibit a higher J_{SC} value than that of PCBM, which is probably due to their more efficient electron extraction. Fig. 2e shows the J–V curves of devices based on polymeric ETLs scanning from forward and reverse directions. The J–V curves of different scanning directions are nearly overlapped, suggesting

negligible hysteresis in the devices.[43] The PCE distribution of different ETLs is displayed in Fig. 2f.

The film morphologies of ETLs coated upon the perovskite layer are of important significance for the performance of PSCs. Therefore, scanning electron microscopy (SEM) was conducted to characterize the film morphologies of perovskite and ETLs coated on perovskite. It was found that the perovskite layer (Fig. 3a) exhibited a dense crystal packing and rough surface, and pinholes can be seen after coating with PCBM (Fig. 3b), which could be caused by aggregation. Meanwhile, more uniform surfaces (Fig. 3c–e) were displayed after coating with polymeric ETLs. Fig. 3f presents the cross-section SEM image of the ITO/PTAA/MAPbI$_3$/P(DTCDI-2T)/BCP/Ag device, confirming good coverage of ETLs on perovskite, and clearly shows its layered structure. Atomic force microscopy (AFM) was also performed to characterize the surface condition of various films. Fig. S4 (ESI†) shows the AFM images of the as-prepared perovskite films, and the PCBM, P(DTCDI-T), P(DTCDI-2T), and P(DTCDI-3T) covered perovskite films. Large dense grains can be seen from the as-prepared perovskite film, giving a root-mean-square (RMS) roughness of 25.2 nm. After coating different ETLs upon the perovskite layer, the RMS roughness decreased to 19.9, 8.5, 14.6, and 8.9 nm for PCBM, P(DTCDI-T), P(DTCDI-2T), and P(DTCDI-3T) covered films, respectively. The decrease of RMS roughness confirms high coverage of ETLs, and the polymeric ETL covered films showed significantly smaller RMS roughness, reflecting their more uniform features and smoother surfaces. The results of AFM characterization are consistent with those of SEM.

Table 2 Photovoltaic parameters of PSC devices based on different ETLs (the data in brackets are the average values among 20 devices)

ETLs	V_{OC} (V)	J_{SC} (mA cm^{-2})	FF (%)	PCE (%)
PCBM	1.08	19.80	72.95	15.56 (14.08 ± 0.87)
P(DTCDI-T)	1.02	23.09	67.16	15.75 (14.04 ± 0.90)
P(DTCDI-2T)	1.06	23.18	73.03	17.88 (16.52 ± 0.83)
P(DTCDI-3T)	1.07	22.84	72.91	17.74 (16.39 ± 0.67)
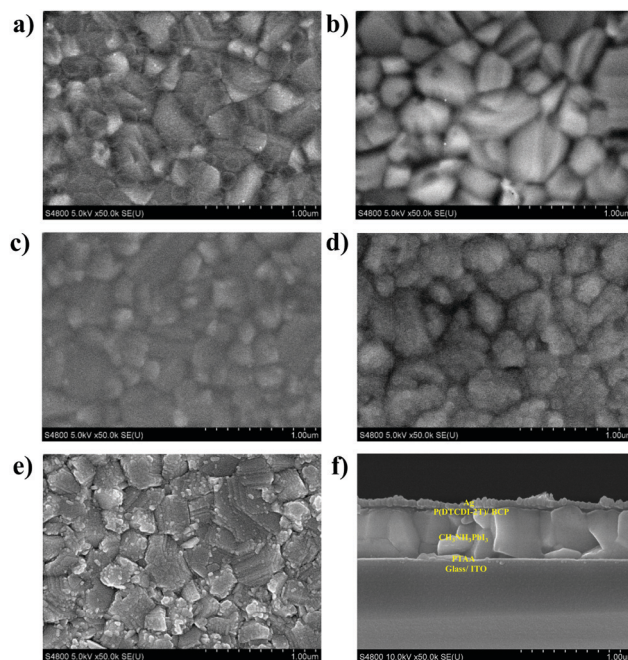
Fig. 3 The SEM images of (a) MAPbI$_3$, (b) MAPbI$_3$/PCBM, (c) MAPbI$_3$/P(DTCDI-T), (d) MAPbI$_3$/P(DTCDI-2T), (e) MAPbI$_3$/P(DTCDI-3T) and (f) cross-section of ITO/PTAA/MAPbI$_3$/P(DTCDI-2T)/BCP/Ag.

This journal is © The Royal Society of Chemistry 2022

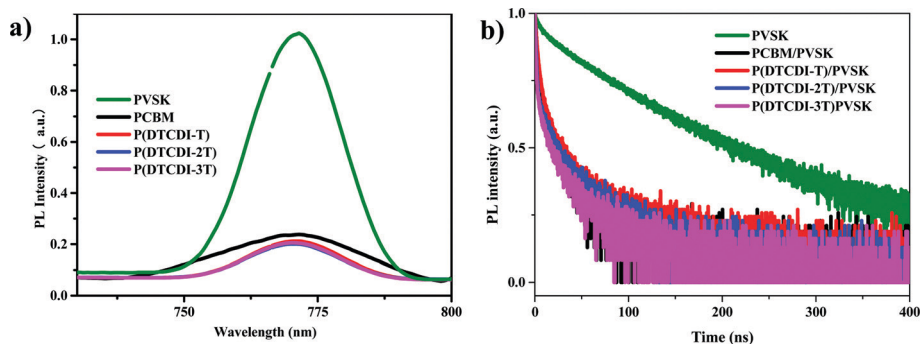*J. Mater. Chem. C*, 2022, **10**, 2703–2710 | **2707**

Fig. 4 (a) Steady-state photoluminescence (PL) spectra, and (b) time-resolved photoluminescence (TRPL) decay traces of the perovskite films (PVSK) and ETL-covered perovskite films.

To investigate the electron extraction properties of the polymer ETLs, steady-state photoluminescence (PL) (Fig. 4a) and time-resolved photoluminescence decay (TRPL) (Fig. 4b) measurements were conducted on the perovskite film and the perovskite films covered with different ETLs. Covering with diverse ETLs would quench the PL intensity of perovskite films, and the percentage of quenching indicates the electron extraction efficiency. Compared to the PCBM-covered perovskite film, the polymer-covered films exhibited distinctly more efficient depression of the PL intensity. This could partly account for their higher J_{SC} values in PSCs. The TRPL decay traces can be fitted by a biexponential decay model, and the given parameters are listed in Table S1 (ESI†). After covering respectively with PCBM, P(DTCDI-T), P(DTCDI-2T) and P(DTCDI-3T), the TRPL lifetime (τ_{ave}) of perovskite films is gradually reduced. The fast decay parameter τ_1, which is typically ascribed to electron extraction, dramatically reduced (396.6 ns for perovskite, and 19.9 ns, 14.9 ns, 2.7 ns, and 3.2 ns after being covered with PCBM, P(DTCDI-T), P(DTCDI-2T) and P(DTCDI-3T) upon perovskite), and P(DTCDI-2T) and P(DTCDI-3T) covered ones display clearly shorter decay time compared with the P(DTCDI-T) one. The reduced lifetime reflects that the electron extraction ability of these polymers is better than that of PCBM, which is in good agreement with the results of steady-state PL measurements, demonstrating their potential as alternatives in constructing efficient PSCs. Moreover, surface trap passivation of perovskite was believed to play an important role in determining the device performance. S atoms within the backbone can possibly work as an electron pair donor to interact with the under-coordinated Pb^{2+}, and thus passivate the possible trap sites on the perovskite film.[37,44,45]

To gain insight into interfacial interaction between the perovskite layer and these polymeric ETLs, we conducted X-ray photoelectron spectroscopy (XPS) measurements, and the recorded results are shown in Fig. S5 (ESI†). For the perovskite film sample, two main peaks located at 138.0 and 142.8 eV were observed, assigned to Pb $4f_{7/2}$ and $4f_{5/2}$, respectively, and there are also two small peaks at 136.4 and 141.3 eV, corresponding to metallic Pb.[46–49] The presence of metallic Pb often acts as electron trap sites, hampering the device efficiency.[46] Interestingly, the metallic Pb signals

disappeared in polymer coated samples, and 0.3 eV shifts toward higher binding energy have been observed for Pb $4f_{7/2}$

Fig. 5 (a) Trap-state densities of PCBM, P(DTCDI-T), P(DTCDI-2T) and P(DTCDI-3T) coated perovskite films. (b) Nyquist plot of impedance spectroscopy for PSCs with PCBM, P(DTCDI-T), P(DTCDI-2T) and P(DTCDI-3T) as an ETL. (c) The stability of devices under ambient conditions.

2708 | *J. Mater. Chem. C*, 2022, **10**, 2703–2710

This journal is © The Royal Society of Chemistry 2022

and $4f_{5/2}$. In S 2p spectra, P(DTCDI-2T) has two peaks at 164.3 and 165.5 eV, which shift to 164.1 and 165.3 eV, respectively, after coating upon perovskite. These results provide direct evidence of strong binding interaction between ETLs and perovskite layer, suggesting effective interface passivation.

The surface trap passivation efficiency can also be compared by quantifying the trap-state density N_{trap}.[50,51] Therefore, devices with the architecture of ITO/SnO$_2$/MAPbI$_3$/ETL/BCP/Ag were made, and their trap-filling-limited voltages (V_{TFL}) were estimated (Fig. 5a) to be 0.26 V, 0.24 V, 0.19 V and 0.24 V for PCBM, P(DTCDI-T), P(DTCDI-2T) and P(DTCDI-3T), respectively. The corresponding trap-state density N_{trap} values were calculated to be 4.55×10^{15}, 4.20×10^{15}, 3.33×10^{15} and 4.20×10^{15} cm^{-3}, respectively. Compared with the PCBM-based device, polymer-based devices bear lower density of electron trap states, which could be due to the better morphology and passivation of defects, and this is consistent with the previous measurements. The lower density of trap states would generate fewer recombination centers and reduce loss in potential.[51] Furthermore, electronic impedance spectroscopy measurements were performed to gain more information on the interfacial charge transport. Fig. 5b shows the Nyquist plots of electrochemical impedance spectroscopy (EIS) for PSCs with different ETLs, and the corresponding data are listed in Table S2 (ESI†). Nyquist plots enable us to discuss the charge transfer process within cells. It is clear that the P(DTCDI-2T) based device has the smallest series resistance (R_s) and charge transfer resistance (R_{ct}), which is aligned with photovoltaic performance data.

Device stability is also an important characteristic to evaluate the performance of PSCs. As shown in Fig. 5c, compared with devices based on the PCBM ETL, all the polymeric ETL based devices exhibited considerably improved stability. It shows that the devices with a P(DTCDI-2T) ETL maintained 87% of their initial efficiency after storing for 168 h, while the PCBM ones maintained 81% of their initial efficiency. The passivation effect of P(DTCDI-2T) could likely account for device stability. Moisture-induced decomposition of the perovskite layer is a crucial destabilization factor for PSCs.[52–55] We tested the contact angles of water droplets on PCBM, P(DTCDI-T), P(DTCDI-2T) and P(DTCDI-3T) thin films. As displayed in Fig. S6 (ESI†), the P(DTCDI-T), P(DTCDI-2T) and P(DTCDI-3T) show hydrophobic contact angles of 99.5°, 100.5° and 100.4°, while PCBM is relatively hydrophilic (contact angle against water of 80.4°). The hydrophobicity of these polymeric ETLs is certainly favorable for suppressing moisture-induced instability.

Conclusions

To summarize, we designed and synthesized a series of DTCDI-based n-type polymers P(DTCDI-T), P(DTCDI-2T) and P(DTCDI-3T) and explored their application as ETLs in PSCs. The ratio of thiophene units within the polymeric backbone has a notable impact on the optical, electrochemical and electron extraction and transport properties, as well as the photovoltaic performance. Thanks to efficient electron extraction, efficient

interfacial electron transport and low interfacial impedance, the PSC devices with the P(DTCDI-2T) ETL resulted in a higher short-circuit current and improved fill factor and displayed a champion power conversion efficiency of up to 18%, which is among one of the highest PCE values of PSCs with a polymeric ETL. Additionally, due to the more hydrophobic feature, the devices with P(DTCDI-T), P(DTCDI-2T) and P(DTCDI-3T) ETLs displayed ameliorated device stability compared to PCBM based devices. These results demonstrate the great potential of DTCDI-based conjugated polymers as efficient ETLs for high-performance PSCs. Our research also provides a rational way to effectively develop polymeric ETLs for PSCs by variation of donor ratios of D–A polymers.

Conflicts of interest

There are no conflicts to declare.

Acknowledgements

Notes and references

1 A. Kojima, K. Teshima, Y. Shirai and T. Miyasaka, *J. Am. Chem. Soc.*, 2009, **131**, 6050–6051.

2 H.-S. Kim, C.-R. Lee, J.-H. Im, K.-B. Lee, T. Moehl, A. Marchioro, S.-J. Moon, R. Humphry-Baker, J.-H. Yum, J. E. Moser, M. Grätzel and N.-G. Park, *Sci. Rep.*, 2012, **2**, 591.

3 M. M. Lee, J. Teuscher, T. Miyasaka, T. N. Murakami and H. J. Snaith, *Science*, 2012, **338**, 643–647.

4 W. S. Yang, B.-W. Park, E. H. Jung, N. J. Jeon, Y. C. Kim, D. U. Lee, S. S. Shin, J. Seo, E. K. Kim, J. H. Noh and S. I. Seok, *Science*, 2017, **356**, 1376–1379.

5 E. H. Jung, N. J. Jeon, E. Y. Park, C. S. Moon, T. J. Shin, T.-Y. Yang, J. H. Noh and J. Seo, *Nature*, 2019, **567**, 511–515.

6 Q. Jiang, Y. Zhao, X. Zhang, X. Yang, Y. Chen, Z. Chu, Q. Ye, X. Li, Z. Yin and J. You, *Nat. Photonics*, 2019, **13**, 460–466.

7 A. K. Jena, A. Kulkarni and T. Miyasaka, *Chem. Rev.*, 2019, **119**, 3036–3103.

8 S. D. Stranks, G. E. Eperon, G. Grancini, C. Menelaou, M. J. P. Alcocer, T. Leijtens, L. M. Herz, A. Petrozza and H. J. Snaith, *Science*, 2013, **342**, 341–344.

9 J. Y. Kim, J.-W. Lee, H. S. Jung, H. Shin and N.-G. Park, *Chem. Rev.*, 2020, **120**, 7867–7918.

10 H. Zhou, Q. Chen, G. Li, S. Luo, T.-B. Song, H.-S. Duan, Z. Hong, J. You, Y. Liu and Y. Yang, *Science*, 2014, **345**, 542–546.

11 M. Graetzel, R. A. J. Janssen, D. B. Mitzi and E. H. Sargent, *Nature*, 2012, **488**, 304–312.

This journal is © The Royal Society of Chemistry 2022

J. Mater. Chem. C, 2022, **10**, 2703–2710 | 2709

12 S. Wang, T. Sakurai, W. Wen and Y. Qi, *Adv. Mater. Interfaces*, 2018, **5**, 1800260.

13 M. Cheng, C. Chen, X. Yang, J. Huang, F. Zhang, B. Xu and L. Sun, *Chem. Mater.*, 2015, **27**, 1808–1814.

14 H. Chen, D. Bryant, J. Troughton, M. Kirkus, M. Neophytou, X. Miao, J. R. Durrant and I. McCulloch, *Chem. Mater.*, 2016, **28**, 2515–2518.

15 M. Saliba, S. Orlandi, T. Matsui, S. Aghazada, M. Cavazzini, J.-P. Correa-Baena, P. Gao, R. Scopelliti, E. Mosconi, K.-H. Dahmen, F. De Angelis, A. Abate, A. Hagfeldt, G. Pozzi, M. Graetzel and M. K. Nazeeruddin, *Nat. Energy*, 2016, **1**, 15017.

16 B. Xu, J. Zhang, Y. Hua, P. Liu, L. Wang, C. Ruan, Y. Li, G. Boschloo, E. M. J. Johansson, L. Kloo, A. Hagfeldt, A. K. Y. Jen and L. Sun, *Chem*, 2017, **2**, 676–687.

17 J. A. Christians, P. Schulz, J. S. Tinkham, T. H. Schloemer, S. P. Harvey, B. J. Tremolet de Villers, A. Sellinger, J. J. Berry and J. M. Luther, *Nat. Energy*, 2018, **3**, 68–74.

18 Q.-Q. Ge, J.-Y. Shao, J. Ding, L.-Y. Deng, W.-K. Zhou, Y.-X. Chen, J.-Y. Ma, L.-J. Wan, J. Yao, J.-S. Hu and Y.-W. Zhong, *Angew. Chem., Int. Ed.*, 2018, **57**, 10959–10965.

19 Z. Yao, F. Zhang, Y. Guo, H. Wu, L. He, Z. Liu, B. Cai, Y. Guo, C. J. Brett, Y. Li, C. V. Srambickal, X. Yang, G. Chen, J. Widengren, D. Liu, J. M. Gardner, L. Kloo and L. Sun, *J. Am. Chem. Soc.*, 2020, **142**, 17681–17692.

20 J. Lian, B. Lu, F. Niu, P. Zeng and X. Zhan, *Small Methods*, 2018, **2**, 1800082.

21 E. Castro, J. Murillo, O. Fernandez-Delgado and L. Echegoyen, *J. Mater. Chem. C*, 2018, **6**, 2635–2651.

22 L.-L. Deng, S.-Y. Xie and F. Gao, *Adv. Electron. Mater.*, 2018, **4**, 1700435.

23 D. Luo, W. Yang, Z. Wang, A. Sadhanala, Q. Hu, R. Su, R. Shivanna, G. F. Trindade, J. F. Watts, Z. Xu, T. Liu, K. Chen, F. Ye, P. Wu, L. Zhao, J. Wu, Y. Tu, Y. Zhang, X. Yang, W. Zhang, R. H. Friend, Q. Gong, H. J. Snaith and R. Zhu, *Science*, 2018, **360**, 1442–1446.

24 S.-K. Jung, D. S. Lee, M. H. Ann, S. H. Im, J. H. Kim and O. P. Kwon, *ChemSusChem*, 2018, **11**, 3882–3892.

25 L. Meng, J. You, T.-F. Guo and Y. Yang, *Acc. Chem. Res.*, 2016, **49**, 155–165.

26 W. Wang, J. Yuan, G. Shi, X. Zhu, S. Shi, Z. Liu, L. Han, H.-Q. Wang and W. Ma, *ACS Appl. Mater. Interfaces*, 2015, **7**, 3994–3999.

27 C. Sun, Z. Wu, H.-L. Yip, H. Zhang, X.-F. Jiang, Q. Xue, Z. Hu, Z. Hu, Y. Shen, M. Wang, F. Huang and Y. Cao, *Adv. Energy Mater.*, 2016, **6**, 1501534.

28 L. Tian, Z. Hu, X. Liu, Z. Liu, P. Guo, B. Xu, Q. Xue, H.-L. Yip, F. Huang and Y. Cao, *ACS Appl. Mater. Interfaces*, 2019, **11**, 5289–5297.

29 C. Deng, L. Wan, S. Li, L. Tao, S.-N. Wang, W. Zhang, J. Fang, Z. Fu and W. Song, *Org. Electron.*, 2020, **87**, 105959.

30 A. A. Said, J. Xie, Y. Wang, Z. Wang, Y. Zhou, K. Zhao, W.-B. Gao, T. Michinobu and Q. Zhang, *Small*, 2019, **15**, 1803339.

31 H. I. Kim, M.-J. Kim, K. Choi, C. Lim, Y.-H. Kim, S.-K. Kwon and T. Park, *Adv. Energy Mater.*, 2018, **8**, 1702872.

32 K. Jiang, F. Wu, L. Zhu and H. Yan, *ACS Appl. Mater. Interfaces*, 2018, **10**, 36549–36555.

33 Y. Shi, W. Chen, Z. Wu, Y. Wang, W. Sun, K. Yang, Y. Tang, H. Y. Woo, M. Zhou, A. B. Djurišić, Z. He and X. Guo, *J. Mater. Chem. A*, 2020, **8**, 13754–13762.

34 W. Chen, Y. Shi, Y. Wang, X. Feng, A. B. Djurišić, H. Y. Woo, X. Guo and Z. He, *Nano Energy*, 2020, **68**, 104363.

35 X. Zhao, C. Ge, X. Yang and X. Gao, *Mater. Chem. Front.*, 2017, **1**, 1635–1640.

36 X. Zhao, C. Ge, X. Xu, J. Huang, X. Yang, Q. Peng, W.-S. Li and X. Gao, *Chem. Commun.*, 2019, **55**, 10234–10237.

37 N. K. Noel, A. Abate, S. D. Stranks, E. S. Parrott, V. M. Burlakov, A. Goriely and H. J. Snaith, *ACS Nano*, 2014, **8**, 9815–9821.

38 C. M. Cardona, W. Li, A. E. Kaifer, D. Stockdale and G. C. Bazan, *Adv. Mater.*, 2011, **23**, 2367–2371.

39 H. Huang, N. Zhou, R. P. Ortiz, Z. Chen, S. Loser, S. Zhang, X. Guo, J. Casado, J. T. López Navarrete, X. Yu, A. Facchetti and T. J. Marks, *Adv. Funct. Mater.*, 2014, **24**, 2782–2793.

40 J. Clark, J.-F. Chang, F. C. Spano, R. H. Friend and C. Silva, *Appl. Phys. Lett.*, 2009, **94**, 163306.

41 P. Ehrenreich, S. T. Birkhold, E. Zimmermann, H. Hu, K.-D. Kim, J. Weickert, T. Pfadler and L. Schmidt-Mende, *Sci. Rep.*, 2016, **6**, 32434.

42 F. C. Spano and C. Silva, *Annu. Rev. Phys. Chem.*, 2014, **65**, 477–500.

43 Y. Rong, Y. Hu, S. Ravishankar, H. Liu, X. Hou, Y. Sheng, A. Mei, Q. Wang, D. Li, M. Xu, J. Bisquert and H. Han, *Energy Environ. Sci.*, 2017, **10**, 2383–2391.

44 L. Liu, S. Huang, Y. Lu, P. Liu, Y. Zhao, C. Shi, S. Zhang, J. Wu, H. Zhong, M. Sui, H. Zhou, H. Jin, Y. Li and Q. Chen, *Adv. Mater.*, 2018, **30**, 1800544.

45 W. Chen, Y. Wang, G. Pang, C. W. Koh, A. B. Djurišić, Y. Wu, B. Tu, F.-Z. Liu, R. Chen, H. Y. Woo, X. Guo and Z. He, *Adv. Funct. Mater.*, 2019, **29**, 1808855.

46 D. Bi, C. Yi, J. Luo, J.-D. Décoppet, F. Zhang, S. M. Zakeeruddin, X. Li, A. Hagfeldt and M. Grätzel, *Nat. Energy*, 2016, **1**, 16142.

47 H. Cho, S.-H. Jeong, M.-H. Park, Y.-H. Kim, C. Wolf, C.-L. Lee, J. H. Heo, A. Sadhanala, N. Myoung, S. Yoo, S. H. Im, R. H. Friend and T.-W. Lee, *Science*, 2015, **350**, 1222–1225.

48 N. B. Rahna, V. Kalarivalappil, M. Nageri, S. C. Pillai, S. J. Hinder, V. Kumar and B. K. Vijayan, *Mater. Sci. Semicond. Process.*, 2016, **42**, 303–310.

49 R. Lindblad, D. Bi, B.-w. Park, J. Oscarsson, M. Gorgoi, H. Siegbahn, M. Odelius, E. M. J. Johansson and H. Rensmo, *J. Phys. Chem. Lett.*, 2014, **5**, 648–653.

50 K. Chen, P. Wu, W. Yang, R. Su, D. Luo, X. Yang, Y. Tu, R. Zhu and Q. Gong, *Nano Energy*, 2018, **49**, 411–418.

51 K. Poorkazem and T. L. Kelly, *Sustainable Energy Fuels*, 2018, **2**, 1332–1341.

52 B.-A. Chen, J.-T. Lin, N.-T. Suen, C.-W. Tsao, T.-C. Chu, Y.-Y. Hsu, T.-S. Chan, Y.-T. Chan, J.-S. Yang, C.-W. Chiu and H. M. Chen, *ACS Energy Lett.*, 2017, **2**, 342–348.

53 Q. Wang, B. Chen, Y. Liu, Y. Deng, Y. Bai, Q. Dong and J. Huang, *Energy Environ. Sci.*, 2017, **10**, 516–522.

54 L. Zhang, M.-G. Ju and W. Liang, *Phys. Chem. Chem. Phys.*, 2016, **18**, 23174–23183.

55 J. Schlipf, L. Bießmann, L. Oesinghaus, E. Berger, E. Metwalli, J. A. Lercher, L. Porcar and P. Müller-Buschbaum, *J. Phys. Chem. Lett.*, 2018, **9**, 2015–2021.

2710 | *J. Mater. Chem. C*, 2022, **10**, 2703–2710

This journal is © The Royal Society of Chemistry 2022